

Elucidating loessal landslide initiation in wood- and shrub-land by hydro-mechanical heterogeneity

Ruijie Yang, Chao Ma, Xi Yang, Yan Zhang, Liqun Lyu, Xinying Wang

School of Soil and Water Conservation, Beijing Forestry University, Beijing 100083, PR China

Corresponding author: Professor Chao Ma, sanguoxumei@163.com

Abstract: Vegetation recovery on the Chinese Loess Plateau has markedly changed the hydrological and mechanical controls on hillslope erosion, shifting sediment production from runoff-driven erosion to gravity-driven processes such as rainfall-induced loessal landslides. Presently, few studies have clearly documented the differences in landslide erosion and initiation between shrubland and woodland. We conducted field investigations, rainfall soil-moisture observations, dye-tracer experiments, and soil-root tests, to examine landslide characteristics in terms of geometry and volume, excess soil-water ratio, preferential-flow pathways, and failure potential in the two stands. Rainfall-induced loessal landslides in the shrubland stand have shallower failure depths and smaller volumes but are wider than those in the woodland stand, and they are triggered under lower contributing area-slope conditions. Moreover, vertical infiltration in the woodland stand tends to be more stable and efficient, characterized by greater water penetration depth and enhanced pore connectivity. The relationship between the excess soil-water ratio and soil-water storage demonstrates that subsurface flow in woodland stand is triggered at relatively lower degrees of saturation. This behavior is attributed to well-developed preferential-flow pathways and reduced matric suction. The landscape dissection-rainfall index indicates lower landslide susceptibility on steep woodland slopes than on steep shrubland slopes, consistent with the lower landslide density in woodland relative to shrubland. Overall, these hydrological and mechanical contrasts indicate that woodland slopes, by combining deep root systems, stable preferential-flow pathways, and strong mechanical reinforcement, support an effective subsurface flow system that enhances infiltration and delays shallow saturation, thus improving slope stability. These results highlight the need to reassess sediment production on the Loess Plateau by explicitly accounting for landslides rather than attributing it solely to runoff-driven erosion.

Keywords: Shallow landslide; Hillslope hydrology; Landscape dissection-rainfall index

1 Introduction

The Chinese Loess Plateau is one of the most erosive landscapes in the world (Fu et al., 2016; Borrelli et al., 2020; Bai et al., 2024). Since 1980, ecological rehabilitation has significantly improved regional vegetation cover and structure, with vegetation cover now reaching approximately 60% (Feng et al., 2016; Deng et al., 2022; Liao et al., 2025). Restored vegetation, optimized plant community structure, and surface litter accumulation have enhanced water storage capacity and slope stability (Yan et al., 2024; Liu et al., 2025). Since 2010, the region has experienced several rainstorms that are unprecedented in the historical record, as exemplified by storms in 2013, 2017, and 2025 (Tang et al., 2020; Deng et al., 2022; Yang et al., 2023; Hao et al., 2024). Subsequent studies have reported a shift in the dominant erosion process from dispersed runoff erosion to gravitational mass movements (Yang et al., 2024; Du et al., 2025). These findings sufficiently indicate that vegetation recovery on Chinese Loess Plateau alters the dominant sediment-producing processes and soil-erosion patterns.

Vegetation recovery can enhance ecosystem functioning and alter the rainwater infiltration pathways (Gu et al., 2019; Wang et al., 2022; Guan et al., 2024). Increases in surface cover and root penetration significantly enhance rainfall infiltration and promote greater spatial heterogeneity, non-uniform infiltration patterns, and preferential-flow pathways (Li et al., 2007; Zhao et al., 2022). Preferential flow often serves as a primary pathway for rainfall infiltration and can bypass soil-matrix pores to reach deeper soil layers (Bachmair et al., 2012; Franklin et al., 2021).

删除了: However

删除了: two common vegetation types,

删除了: in two steep stands. These data were used

删除了: differences in

删除了:

删除了: that steep woodland slopes have lower landslide susceptibility than steep slopes in shrubland, consistent with the lower susceptibility is consistent with the lower landslide density in woodland than in shrubland

删除了: strongly

52 Preferential flow intensity and morphology vary markedly among vegetation types. Woodland slopes are
53 characterized by deep, continuous macropore channels, predominantly vertical preferential flow, rapid infiltration,
54 and greater deep-soil water storage (Niu et al., 2023; Cai et al., 2024; Zhang et al., 2025). Shrubland slopes exhibit
55 predominantly lateral and diffuse subsurface flow with weak vertical components, thereby retaining much of the
56 infiltrating water in shallow soil layers (Wang et al., 2020; An et al., 2022; Liang et al., 2023; Zhang et al., 2024).
57 Herbaceous slopes rely mainly on surface cracks and earthworm burrows to route water, and therefore preferential
58 flow channels are sparse and discontinuous (Wen et al., 2020; Niu et al., 2023; Li et al., 2025). Vegetation recovery
59 has significantly restructured the soil bio-pore system through root penetration, thereby facilitating the development
60 of preferential-flow pathways and making infiltration regimes more heterogeneous (Zhao et al., 2022; Guan et al.,
61 2024). However, preferential-flow infiltration on steep slopes, particularly at landslide sites with different vegetation
62 types, has not been adequately investigated. During heavy storms, preferential flow can regulate spatiotemporal
63 subsurface water dynamics and act as a biologically mediated control on slope stability.

64 Root morphology and spatial configuration influence rainwater infiltration pathways and soil-moisture
65 redistribution (Fan et al., 2020; Li et al., 2023). On the Chinese Loess Plateau, two predominant vegetation types are
66 recognized: woodlands dominated by *Robinia pseudoacacia* and *Pinus tabulaeformis*, and shrublands dominated by
67 *Rosa xanthina* and *Hippophae rhamnoides*. Woodland trees typically develop deeply penetrating root systems,
68 forming continuous macropore networks and vertical preferential-flow pathways (Zhao et al., 2022; Cai et al., 2024;
69 Wang and Zhang, 2024). These structures facilitate rapid rainfall infiltration into deep soil layers, enhance subsurface
70 moisture retention, delay surface saturation, and reduce surface runoff (Souza et al., 2023; Cai et al., 2024; Hu et al.,
71 2025). In contrast, shrubs develop a dense, fibrous root matrix that promotes mesopores and capillaries formation,
72 thereby accelerating the formation of subsurface saturation zones and limiting vertical percolation (Laycock et al.,
73 1967; Souza et al., 2023; Xiao et al., 2024; Yamase et al., 2024). Therefore, plant roots can control preferential-flow
74 patterns and alter hillslope hydrology. However, few studies have examined how the hydrological effects of mature
75 vegetation influence landslides on the Chinese Loess Plateau.

76 To examine the hydrological and mechanical heterogeneity in mature woodland and shrubland stands on steep
77 slopes and its implications for slope stability, we first analyze landslide geometry and landscape dissection for slides
78 triggered by a low-intensity storm from 3 to 6 October 2021. Then, we assess hydrological heterogeneity in mature
79 woodland and shrubland using soil-moisture observations, excess soil-water ratios across different soil-water storage
80 levels, and preferential-flow pathway identification. Mechanical heterogeneity is characterized by soil and root
81 strength parameters, the soil water characteristic curve (SWCC), and the hydraulic conductivity function (HCF).
82 Finally, we evaluate slope failure potential in relation to landslide density in the two stands. This study mainly
83 addresses the role of vegetation in modulating slope stability by analyzing real landslide cases. Our findings highlight
84 the dual role of vegetation in mitigating landslide erosion and provide new insights into its nuanced effects on
85 hillslope stability.

86 2. Research background

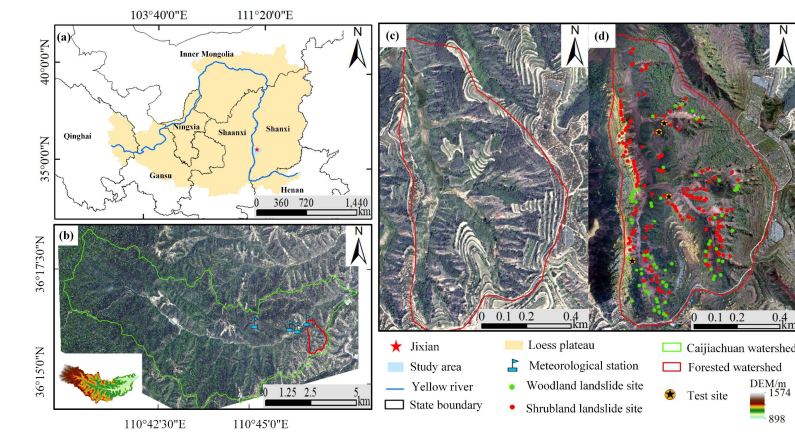
87 2.1 Study area

88 The study area lies in a forested catchment on the southeastern Loess Plateau in China (Fig. 1a). It is located in
89 the downstream reach of the Caijiachuan watershed in Jixian County, Shanxi Province (Fig. 1b). The soil has an
90 unconsolidated, porous structure. On steep slopes, woodland is dominated by *Robinia pseudoacacia* and shrubland
91 by *Rosa xanthina*. Since the farmland reforestation policy was implemented in 1980, forest cover has recovered to
92 about 70%. During 1990–1995 and 1999–2002, the Mountain Improvement Technology Training Project enhanced
93 forest regeneration. Currently, the local soil and water conservation measures serve as a benchmark within the Loess

删除了: soil

95 Plateau region. The area has four distinctive seasons and a cold semi-arid climate. The annual precipitation is
 96 approximately 579.1 mm, and the mean annual temperature is 9.9°C. Most rain events occurs from June to September,
 97 accounting for more than 70% of the annual precipitation. Prior to the 2021 event, a short-duration storm on 25–26
 98 August 2003 triggered 18 landslides, with antecedent precipitation of 71.7 mm over 18 hours and an intense 3 h
 99 rainfall of 24.4 mm (Wang et al., 2024). In contrast, the 2021 rainfall event was a low-intensity storm with prolonged
 100 antecedent precipitation of 121.8 mm over 72 hours and a 6 h peak rainfall of 32.2 mm (Fig. 2). After the storm,
 101 post-storm documentation mainly focused on differences in landslide numbers, densities, slope aspects, and
 102 morphological metrics (Tang et al., 2023), while giving little attention to the hydrological and mechanical conditions
 103 of landslides in the two forested land types.

104
 105 **Figure 1.** Geographical setting of the study area, with the (a) location of Caijiachuan watershed in the Loess Plateau,
 106 China, (b) the forested catchment and meteorological stations in downstream reach of Caijiachuan watershed, (c)
 107 0.15 m resolution orthoimage on 12 October 2019, and (d) 0.10 m resolution orthoimage on 14 October 2021
 108 showing the sites for soil-moisture observations and dye-tracer experiments.



109
 110

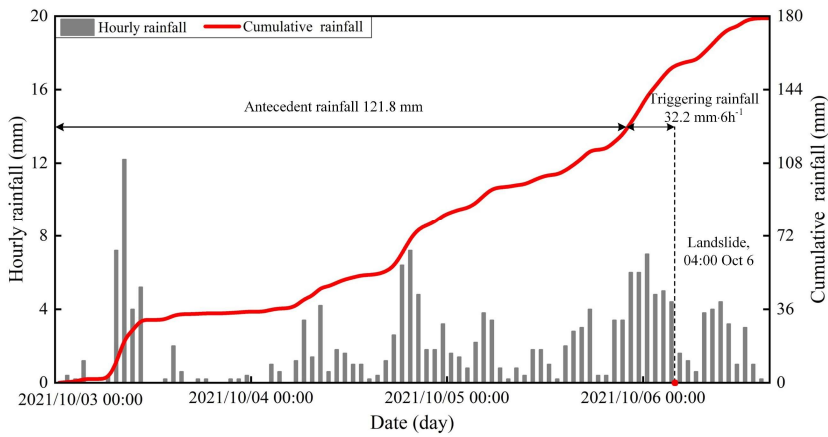


Figure 2. Hourly and cumulative rainfall from 3 to 6 October 2021.

删除了: study

删除了: lies in the transition zone between semi-humid and semi-arid climates

删除了: , with a mean annual temperature of 9.9°C and a mean annual precipitation of 579.1 mm.

删除了: fall

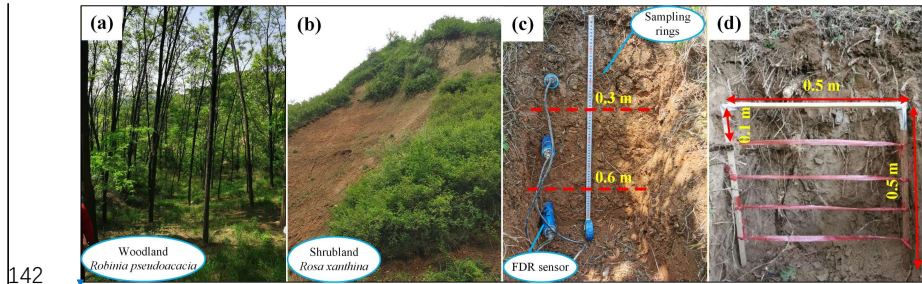
117 **3 Materials and methods**

118 **3.1 Landslide information interpretation**

119 To obtain landslide inventories for the woodland and shrubland, we acquired high-resolution orthoimages and
120 digital elevation models (DEMs) using an unmanned aerial vehicle (UAV; DJI Inspire 2). Two systematic UAV
121 flights with consistent flight and image overlap settings were conducted on 12 October 2019 (Fig. 1c) and 14 October
122 2021 (Fig. 1d). Pix4Dmapper (version 4.6, Pix4D SA, Switzerland) was used to generate ortho-mosaics and DEMs.
123 These DEMs have spatial resolutions of 0.15 m and 0.10 m, respectively, thereby supporting accurate landslide
124 mapping. Landslide point and areal densities are calculated by dividing the total number of landslides and the total
125 scar area by the woodland and shrubland areas, respectively. The lateral extent of each landslide is the sum of the
126 sidewall and head scarp areas. The unit upslope contribution area is the ratio of the total contributing area to the scar
127 width. Slope gradients and associated unit contributing areas are computed from the DEM generated on 14 October
128 2021.

129 **3.2 Rainfall, soil-moisture monitoring and sample collection**

130 In the study area, the woodland has an open structure due to sparse-to-moderate tree density and high canopy
131 height (Fig. 3a), whereas the shrubland has a closed structure because of high density and low canopy height (Fig.
132 3b). Each study site is dominated by single woody species, with *Robinia pseudoacacia* in the woodland and *Rosa*
133 *xanthina* in the shrubland. Both land types have a well-developed herbaceous layer. To investigate the hillslope
134 hydrology, we used frequency-domain reflectometry (FDR) soil-moisture sensors installed at depths of 30, 60, and
135 90 cm to record volumetric water content from May to August 2023 (Fig. 3c). A meteorological station at
136 Caijiachuan Forest Station is approximately 2 kilometers to the northwest of the study area. During soil-moisture
137 sensor installation, we collected undisturbed soil samples near the FDR sensor locations. Bulk density, porosity,
138 effective cohesion, internal friction angle, and unsaturated hydraulic properties were determined using an electronic
139 balance, an oven, a GDS triaxial apparatus, and transient release and imbibition tests (Lu and Godt, 2013). Plant
140 roots were collected to determine depth-dependent root distribution (Fig. 3d), root diameter, root area ratio, and
141 tensile strength (Nimmo et al., 2009).



142 **Figure 3.** Soil moisture monitoring and soil and root sampling. (a) Open woodland dominated by *Robinia*
143 *pseudoacacia*. (b) Close-structure shrubland dominated by *Rosa xanthina*. (c) Trench wall showing soil sampling and FDR sensor
144 installation. (d) In situ root counting and sampling at 0.1 m depth intervals.

146 **3.3 Excessive soil water due to preferential flow**

147 Previous studies of preferential flow on the Loess Plateau have shown that continuous channels in woodland
148 enhance deep soil water storage, whereas lateral and dispersed channels in shrubland keep water in shallow soil
149 layers (Wang et al., 2019; An et al., 2022). Therefore, differences in preferential-flow pathways can result in distinct
150 soil-moisture responses during the same rainfall event. In this study, we first characterized preferential-flow

删除了: Pix4D software

删除了: respective

删除了: Landslide

删除了:

删除了: sparse

删除了:

设置了格式: 字体: 倾斜

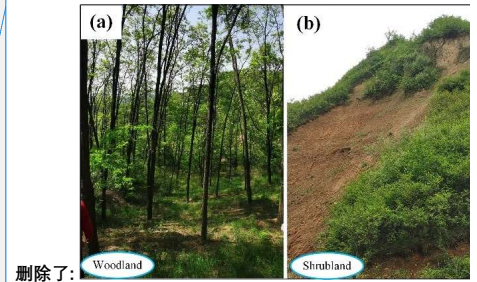
设置了格式: 字体: 倾斜

删除了: located about

删除了: m

删除了: from the study area. Both soil moisture and rainfall were recorded at 5-min intervals

删除了: soil



删除了:

删除了:

164 pathways using dye tracer experiments and then examined soil moisture responses using observed soil moisture data.
 165 Dye tracer experiments were conducted on vegetated slopes near the soil moisture monitoring sites to examine
 166 the preferential flow pathways (Fig. 1d). The slope angles were 35.8° at the woodland site and 38.2° at the
 167 shrubland site. An electric sprayer was used to spray a 4 g·L⁻¹ brilliant blue solution onto a 100 cm × 100 cm plot
 168 (Figs. 4a and 4b). After spraying the solution, the plot was immediately covered with a rainproof cloth to minimize
 169 evaporation. After 24 h, a 5 cm-wide margin of soil was removed from the plot edges, and the core area was
 170 excavated to obtain 10 vertical and 5 horizontal profiles. Excavation grids were established at 0.1 m intervals in both
 171 the longitudinal and transverse directions (Figs. 4c and 4d). Profile images were captured with a digital camera at a
 172 fixed distance and in a parallel orientation, and subsequently processed using Adobe Photoshop (version 2021;
 173 Adobe Inc., USA) and Image-Pro Plus (version 6.0; Media Cybernetics, USA). The proportion of flow marked by
 174 the dye is:

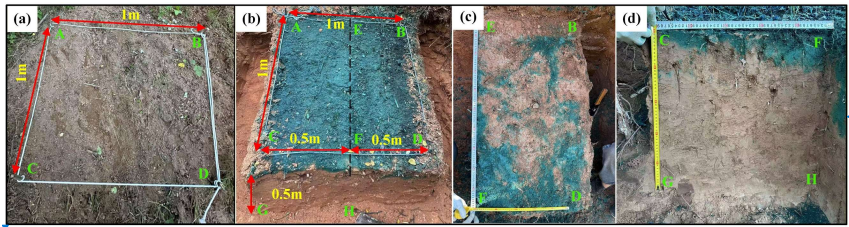
$$SAR = \frac{a_j}{A_j} \quad (1)$$

176 where SAR is the stained-area ratio for the soil profile, j is soil depth (cm), a is the number of stained pixels at
 177 depth j , and A is the total number of pixels along the image width at depth j .

178 The soil moisture response index describes excess soil water in response to a given rainfall input:

$$R_C = \frac{R_{max} - (R + R_0)}{R + R_0} \quad (2)$$

180 where R_C is the excess soil-water ratio in response to a given rainfall event, R_{max} is the maximum total soil-water
 181 storage during the rainfall episode (mm), R is the cumulative rainfall during the episode (mm), and R_0 is the initial
 182 total soil-water storage before the rainfall episode (mm). Positive or negative values of R_C indicate whether the
 183 increase in soil-water storage exceeds or falls below the rainfall input. In addition, R_C reflects the preferential-flow
 184 component aligned with slope orientation or gravity. As soil moisture typically lags rainfall, we follow the method
 185 proposed by Lu et al. (Lu et al., 2024), which defines rainfall episodes using soil depth and in situ saturated hydraulic
 186 conductivity measurements. Therefore, the R_C values under different $R + R_0$ conditions, together with the
 187 preferential-flow pathways, can reflect heterogeneity in soil-water movement in the woodland and shrubland.



188
 189 **Figure 4.** Dye tracer experiments and preferential flow pathways examination. (a) Experimental plot after vegetation
 190 removal. (b) Experimental plot after 24 h of brilliant blue solution spraying. (c) Dye-stained profile parallel to the
 191 slope surface. (d) Dye-stained profile along the gravity direction. Capital letters denote corresponding points shared
 192 across Fig. 4 a - d.

193 3.4 Slope resistance to failure probability at given rainfall input

194 Hillslope resistance to failure at a given rainfall input depends on the topography and the physical, strength,
 195 and hydraulic properties of soil mass. A widely used combination of the infinite-slope stability model and a
 196 hydrological model yield an expression for the critical drainage area per unit contour length (Montgomery and
 197 Dietrich, 1994):

删除了:

删除了:

删除了: in the two land types

删除了:

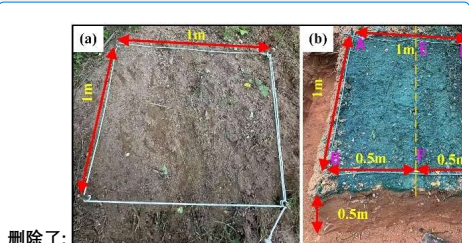
删除了: with

删除了: Photoshop CS and Image-Pro Plus

删除了: /was quantified as

删除了:

删除了: s



删除了:

带格式的: 居中

删除了: Horizontal dye-stained profile.

删除了: Transverse dye-stained profile.

210
$$a_{cr} = \frac{zK\sin\theta\cos\theta}{R_t} \left[\frac{C' + C_r}{\rho_w g z \cos^2 \theta \tan\phi} + \frac{\rho_s}{\rho_w} \left(1 - \frac{\tan\theta}{\tan\phi} \right) \right] \quad (3)$$

211 where a_{cr} is the critical drainage area per unit contour length ($\text{m}^2 \cdot \text{m}^{-1}$), R_t is the triggering rainfall rate ($\text{m} \cdot \text{d}^{-1}$),
 212 K is the saturated hydraulic conductivity ($\text{m} \cdot \text{d}^{-1}$), θ is the slope angle ($^\circ$), C' and C_r are the effective soil
 213 cohesion and the root-induced cohesion (kPa), ρ_s and ρ_w are the unit weights of soil and water ($\text{KN} \cdot \text{m}^{-3}$), z is
 214 the soil thickness (m), and ϕ is the effective internal friction angle ($^\circ$).

215 The left-hand side of Eq. (3) represents the topographic condition of a given landslide or a site susceptible to
 216 slope failure (Montgomery et al., 2000). Moving R_t to the left-hand side yields the right-hand side of Eq. (4) in an
 217 integrated form involving only soil mass parameters:

218
$$a_{cr} \times R_t = \frac{K \tan\theta (C' + C_r)}{\rho_w g \tan\phi} + zK\sin\theta\cos\theta \frac{\rho_s}{\rho_w} \left(1 - \frac{\tan\theta}{\tan\phi} \right) \quad (4)$$

219 The physical meaning of $a_{cr} \times R_t$ is that hillslope resistance to failure under site-specific topographic conditions
 220 and a given rainfall input strongly depends on soil physical properties. For the rain-induced loessal landslides in the
 221 study area, the strength and hydraulic properties of the landslide mass in woodland and shrubland may lead to
 222 different $a_{cr} \times R_t$ levels, so that landslide density (or number) differs between woodland and shrubland. Therefore,
 223 we focus on $a_{cr} \times R_t$ from the right-hand side of Eq. (4) to elucidate the initiation of loessal landslides in two
 224 forested land types.

225 4 Results

226 4.1 Landslides in the two lands

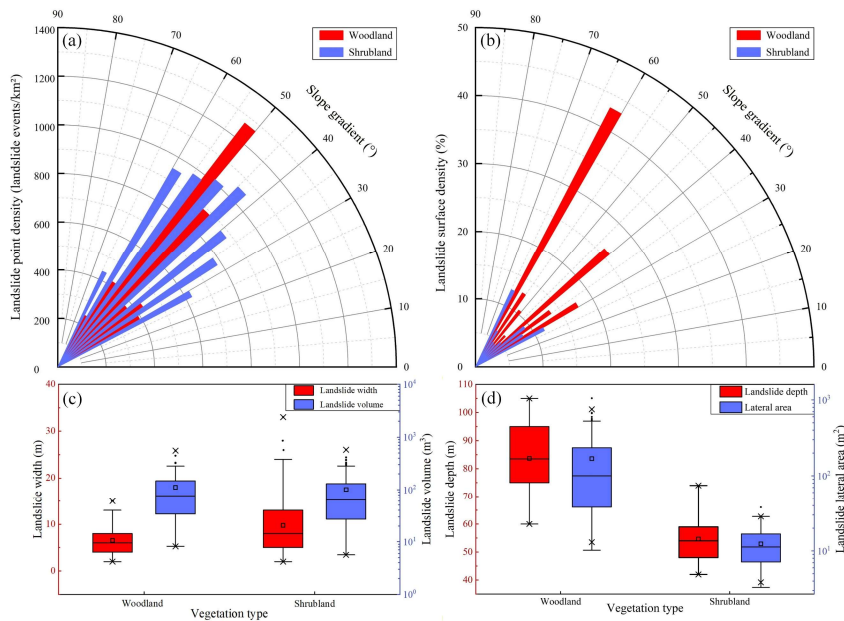
227 To compare the landslide point and areal densities between the two stands, we calculated landslide counts and
 228 areas and divided them by the total steep-terrain area in each stand. This approach excluded non-susceptible terrain
 229 from the analysis. The spatial distribution and morphology of landslides in woodland and shrubland exhibited clear
 230 patterns. Specifically, the statistical results showed that landslide point density in shrubland was 1.56 times that in
 231 woodland, whereas landslide areal density was only 0.48 times that in woodland (Figs. 5a and 5b). Furthermore, the
 232 average landslide width in shrubland was 1.49 times that in woodland. Generally, trees in woodlands have deep root
 233 systems that provide stronger anchoring and can mobilize deeper soil layers, thereby modifying the failure depth
 234 and geometry of shallow landslides (Schwarz et al., 2010; Masi et al., 2023; Dibiagio et al., 2024). The average
 235 landslide depth in woodland was 1.82 times that in shrubland, while the average lateral extent was 1.61 times that in
 236 shrubland. However, the average width of landslides in woodland was only 0.67 times that in shrubland. Overall,
 237 the total landslide volume in woodland was 1.16 times that in shrubland, indicating that landslides in woodland tend
 238 to be larger (Figs. 5c and 5d).

239 When landslides are considered alongside other landscape-dissection agents such as rills and gullies, their
 240 spatial locations depend on two controls. One is spatial competition between the slope-dependent term $S = \tan\theta$ ($\text{m} \cdot \text{m}^{-1}$)
 241 and the area-dependent term A ($\text{m}^2 \cdot \text{m}^{-1}$); the other is exceedance of the A - S topographic threshold (Montgomery
 242 and Dietrich, 1994). As highlighted in Sect. 3.4, variations in $a_{cr} \times R_t$ arise from the interplay of topography, failure
 243 depth, soil strength, plant root reinforcement, and hydraulic conductivity. To evaluate these controls on landslides,
 244 we compared the upslope contributing area (A) and slope gradient (S) between the two land types.

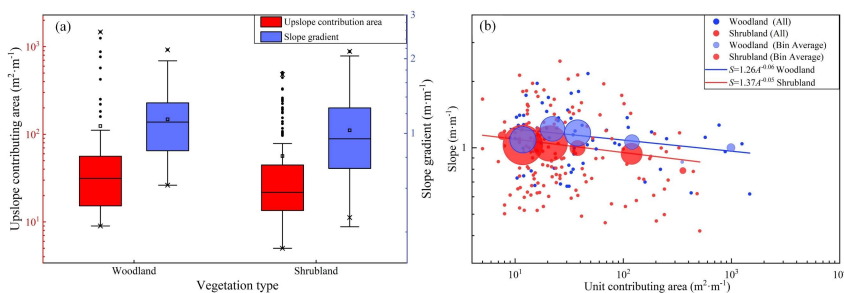
245 Field investigations reveal that most landslides in the study area occur in concave topographic positions.
 246 Statistical analysis indicates that, on average, woodland sites have a significantly larger upslope contributing area
 247 ($124 \text{ m}^2 \cdot \text{m}^{-1}$) and steeper slopes (48°) than shrubland sites. These values are consistent with expectations from the
 248 A - S threshold framework (Fig. 6a). Fitting regression lines to the bin-averaged dataset further demonstrates that
 249 landslides in woodland generally require either a larger upslope contributing area or a steeper slope gradient for

删除了: R_t

251 initiation (Fig. 6b). The $A-S$ relationship shows that, at similar slope gradients, landslides in woodland require larger
 252 upslope contributing areas than those in shrubland. This suggests that, compared with landslides in shrubland, those
 253 in woodland may require higher rainfall-intensity thresholds, steeper slopes, or both, for initiation. Consistent with
 254 this, shrubland shows a higher landslide point density than woodland (1.56 times; Fig. 5a)

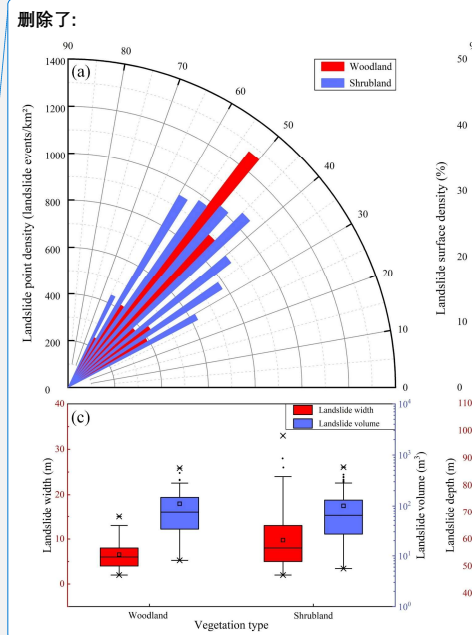


255
 256 **Figure 5.** Landslide characteristics in woodland and shrubland. (a) point density by slope-gradient class; (b) areal
 257 density by slope-gradient class; (c) landslide depth and lateral area; and (d) landslide width and volume. The three
 258 horizontal-lines of box show decreasing order of 75th quantile (Q_3), median (Q_2), and 25th quantile (Q_1). The box
 259 length is the interquartile range ($IQR=Q_3-Q_1$). The small square is the average value. The cross symbols denote the
 260 1st and 99 th percentiles. The upper and lower limit of whiskers are $Q_3+1.5IQR$ and $Q_1-1.5IQR$, respectively. The
 261 whiskers extend to the most extreme values within these limits; mild outliers are shown as black dots.



262
 263 **Figure 6.** Upslope contributing area and slope gradient condition. (a) upslope contributing area and mean slope as
 264 a function of slope aspect; (b) upslope-contributing area vs. mean slope gradient above the landslide area. The

删除了: As a result, landslide point density in woodland is about 50% lower than in shrubland under similar conditions.



删除了: crossing

删除了: the minimum and maximum values, except for mild outliers, which are shown as black dots.

272 definition of the [boxplots](#) is given in the caption of Fig. 5. Circles indicate mean slopes, with radius proportional to
 273 the number of landslides. A power-law regression is fitted to the bin-averaged data.

删除了: whiskers

274 4.2 Soil Hydrological properties

275 4.2.1 SWCC and HCF curves

276 Extensive research has examined saturated hydraulic conductivity and microstructural properties of loess (Xu
 277 et al., 2021; Li et al., 2023). Given that loess on hillslopes largely remains unsaturated during natural rainfall
 278 infiltration and drainage (Lan et al., 2021; Wei et al., 2022), evaluating unsaturated hydro-mechanical differences
 279 using SWCCs and HCFs is important. Therefore, this approach enables comparison among key parameters—
 280 hydraulic conductivity, matric suction, suction stress, and microstructural properties.

281 Table 1 lists the soil parameters obtained through Hydrus-1D inversion. Based on these parameters, the SWCC
 282 and HCF were plotted for the woodland and shrubland sliding-layer soils (Fig. 7). The results indicate that the pore-
 283 size distribution parameter and saturated hydraulic conductivity are significantly higher for woodland soils than for
 284 shrubland soils. This contrast is evident in both drying and wetting processes. This suggests that the pore system in
 285 woodland soils is dominated by larger pores, which enhance water movement. This pore structure facilitates rainfall
 286 infiltration into the soil. In contrast, shrubland soils contain more micropores that retain more water. This is reflected
 287 in a 3.1% higher residual water content in shrubland soils than in woodland soils. During the drying test, the air-
 288 entry pressures of woodland and shrubland soils are nearly identical. However, during the wetting process, the air-
 289 entry pressure in woodland soils is 0.05 kPa lower than in shrubland soils. This indicates that larger pores in
 290 woodland soils begin to drain and fill with air at lower matric suction. As a result, a continuous gas-phase pathway
 291 forms earlier in woodland soils [at the same matric suction](#) (Figs. 7c and 7d). This promotes air-water exchange and
 292 moisture release, making it less likely for the soil to reach or maintain a high degree of saturation for extended
 293 periods. Therefore, under the same rainfall conditions, shrubland soils have weaker moisture-buffering capacity than
 294 woodland soils, making the soil more prone to becoming highly saturated. This reduces the effective stress and shear
 295 strength of shrubland soils, ultimately reducing slope stability.

删除了: at the same matric suction,

296 During the drying and wetting processes, the difference in saturated water content in shrubland sliding-layer
 297 soil (0.101) is approximately 14.43 times that in woodland sliding-layer soil (0.007). This indicates that the pore
 298 structure in shrubland sliding-layer soil is less stable than in woodland sliding-layer soil. Under extreme drying-
 299 wetting conditions, some pores tend to collapse or rearrange, making it difficult for the soil to maintain its original
 300 pore configuration. The resulting changes in pore structure disrupt water flow paths in shrubland sliding-layer soil,
 301 reducing permeability, weakening water flow, and slowing drainage. These findings are consistent with the stronger
 302 hysteresis observed in the SWCC of shrubland sliding-layer soil compared with that of woodland sliding-layer soil
 303 (Fig. 7a and 7b). They further confirm that woodland sliding-layer soil has a greater capacity for moisture
 304 redistribution.

305 **Table 1.** Parameters describing the soil and water characteristic curve (SWCC) and the hydraulic conductivity
 306 function (HCF) from Hydrus 1D

Parameters	Definition	Woodland	Shrubland
θ_s^d	Saturated water content	0.500	0.480
θ_s^w		0.493	0.379
θ_r	Residual water content	0.055	0.086
n^d	The pore size distribution parameter	1.58	2.19
n^w		1.69	1.88
e^d (KPa ⁻¹)	The inverse of the air entry pressure head	5.461×10^{-3}	6.294×10^{-3}

格式化表格

设置了格式: 字体: 倾斜

删除了: moisture

设置了格式: 字体: 倾斜

设置了格式: 字体: 倾斜

删除了: moisture

设置了格式: 字体: 倾斜

设置了格式: 字体: 倾斜

设置了格式: 字体: 倾斜

α^w (KPa ⁻¹)	0.646	0.596
K_s^d (cm s ⁻¹)	2.3×10^{-5}	5.4×10^{-6}
K_s^w (cm s ⁻¹)	7.1×10^{-2}	5.0×10^{-3}

Notes: Superscripts "d" and "w" denote the drying and wetting processes, respectively.

设置了格式: 字体: 倾斜

设置了格式: 字体: 倾斜

设置了格式: 字体: 倾斜

带格式的: 左, 段落间距段前: 0 磅

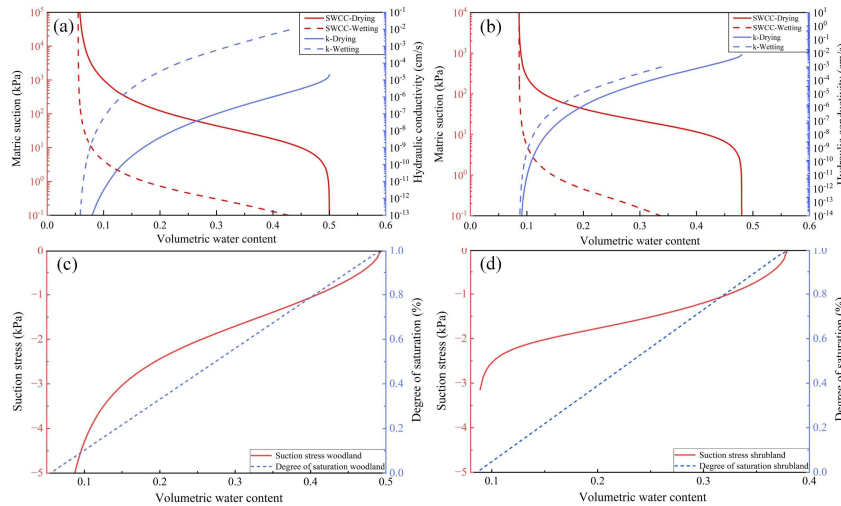


Figure 7. Differences in the hydromechanical properties of the sliding-layer soil. (a) SWCC for layer 3 of the woodland soil profile; (b) SWCC for layer 2 of the shrubland soil profile; (c) Suction stress–volumetric water content curves for layer 3 of the woodland soil profile; (d) Suction stress–volumetric water content curves for layer 2 of the shrubland soil profile.

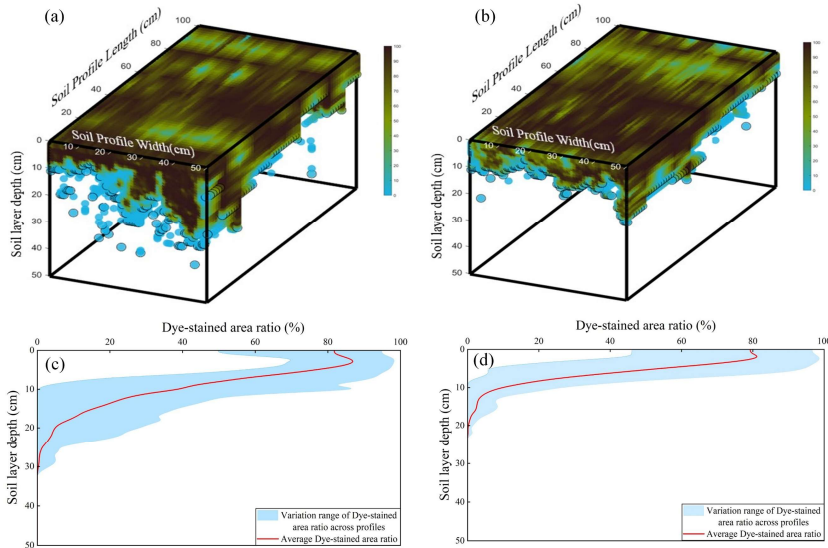
4.2.2 Dye tracer experiments

Dye-tracer experiments directly visualize the flow pathways of water infiltration in woodland and shrubland soils. Under the same applied water volume and infiltration area, the stained soil volume in woodland soils is markedly larger than that in shrubland soils. Three-dimensional visualizations reveal that stained pathways in woodland soils form thick bands with numerous vertically continuous columnar channels. Hydraulic connectivity is high, and water infiltrates to greater depths. Stained bands in shrubland soils are shallow, and vertical, filament-like channels are nearly absent. In addition, the depth-dependent pattern of dye-stained area ratios in the shrubland profile further confirms that vertical infiltration is restricted to relatively shallow depths. Differences in the volume, depth, and morphology of the stained pathways indicate that infiltration in woodland soils no longer follows uniform matrix-flow conditions. This is also evident in the dye-stained areas of vertical profiles. Woodland profiles show large, continuous color patches, whereas shrubland profiles mainly show fragmented spots concentrated in shallow soil. This pattern suggests that deeper shrubland soils are denser and have lower pore connectivity.

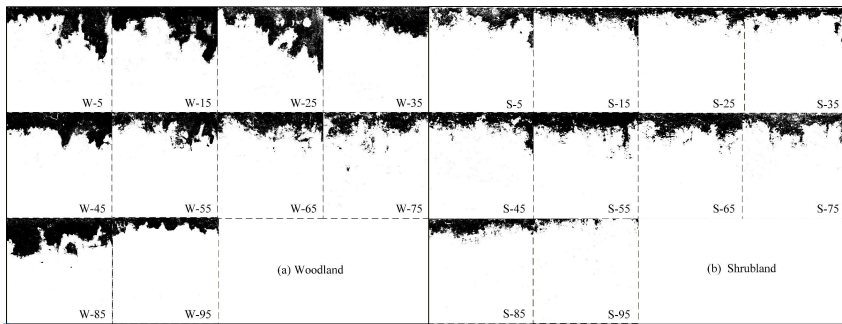
Overall, woodland soils more readily develop a stable, efficient vertical percolation system with greater infiltration depth and stronger connectivity. This promotes deep water storage and redistribution. In contrast, insufficient pore connectivity in shrubland soils causes water to remain in shallow layers, prolonging surface wetness and slowing pore-water pressure recovery. Under intense rainfall, this condition favors saturation buildup and thus increases the likelihood of landslide initiation. This flow pattern is consistent with the SWCC- and HCF-inferred

334 differences in soil hydraulic behavior and provides direct, pathway-scale evidence of flow pathways, which cannot
 335 be resolved from the curve-derived hydraulic parameters alone.

删除了: differences soil-matrix hydraulic behavior differences inferred from SWCC and HCF and provides a path-based complement to traditional hydraulic parameters.



336
 337 **Figure 8.** Morphological characteristics of dye-stained flow paths in woodland and shrubland soils. (a) Three-
 338 dimensional visualization of stained zones in woodland; (b) Three-dimensional visualization of stained zones in
 339 shrubland; (c) Dye-stained area ratio vs. soil depth in woodland; (d) Dye-stained area ratio vs. soil depth in shrubland.



340
 341 **Figure 9.** Schematic dye-stained vertical soil profiles at different hillslope positions. (a) Woodland profile; (b)
 342 Shrubland profile. Numbers from 0 to 100 denote relative slope positions, with lower values indicating locations
 343 near the slope base.

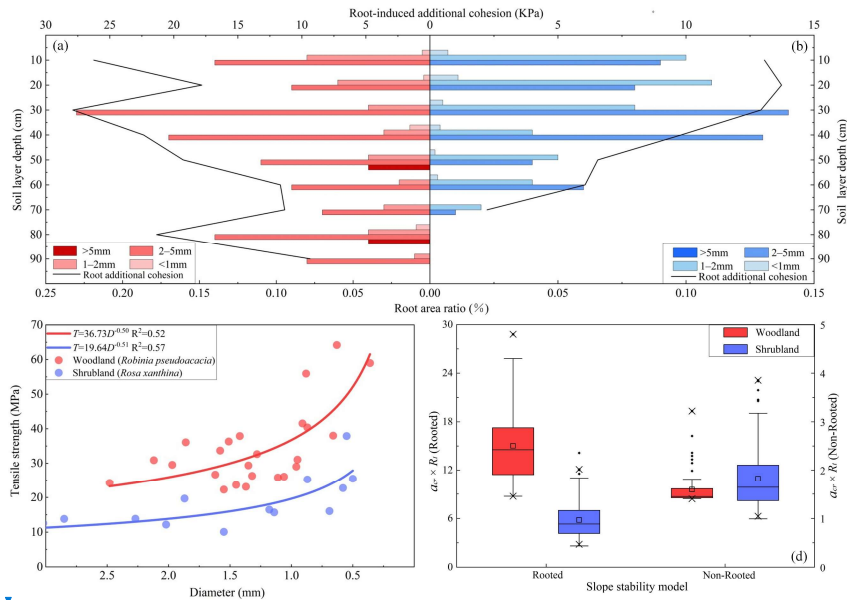
344 **4.3 Slope hydrological characteristics**

345 To characterize how woodland and shrubland soils respond to rainfall, we group rainfall events into distinct
 346 episodes based on soil depth and in rain saturated hydraulic conductivity (Fig. 10a). Using these episodes as the
 347 basic analytical units, we then assess the intensity of slope-surface responses and the associated water distribution.
 348 This approach overcomes the limitations of using rainfall statistics alone. It explicitly addresses the slope's dynamic

删除了: Quantifying how rainfall translates into changes in soil-water content is critical for analyzing rainfall-induced landslides in this region.

删除了: situ

391 Compared with *Rosa xanthina*, roots in *Robinia pseudoacacia* mobilize greater root-induced cohesion at a given
 392 root diameter and exhibit a larger specific root area ratio (RAR). These roots therefore create a more extensive root-
 393 soil contact interface and form a mechanically stronger root-soil composite.



394 **Figure 11.** Mechanical indices of slope stability in woodland and shrubland. (a) Root area ratio and root-induced
 395 cohesion in woodland (*Robinia pseudoacacia*); (b) Root area ratio and root-induced cohesion in shrubland (*Rosa*
 396 *xanthina*); (c) Relationship between root tensile strength and diameter; (d) Slope-stability models for woodland and
 397 shrubland. The definitions of the [boxplots](#) given in the caption of Fig. 5.

399 Using the parameters in Table 2, we constructed a slope stability model to evaluate slope resistance to failure
 400 under specified topographic conditions and rainfall inputs. When root-induced cohesion is ignored, mean $a_{cr} \times R_t$
 401 values in woodland and shrubland are similar, indicating that slope stability differs little between them. When root
 402 effects are included, slope stability increases markedly. In woodland, the $a_{cr} \times R_t$ value rises to 15.02,
 403 approximately 338% higher than in shrubland (Fig. 11d). These results indicate that woodland roots contribute much
 404 more to slope stability than roots in shrubland. Woodland roots substantially increase the critical rainfall and
 405 topographic thresholds for landslide initiation and confirm the key role of roots in strengthening slopes and resisting
 406 landslide-triggering factors.

407 **Table 2** Parameters describing the slope stability model

Parameters	Definition	Woodland	Shrubland
ρ_s ($\text{kg} \cdot \text{m}^{-3}$)	Dry soil density	1.37	1.41
θ ($^\circ$)	Slope gradient	31.71–65.27	22.78–67.96
C' (kPa)	Effective soil cohesion	5.97	7.35
C_r (kPa)	Root-induced cohesion	18.59	10.36
φ ($^\circ$)	Effective friction angle	18.67	14.50
z (m)	Landslide depth	0.84	0.54

删除了: shrubland

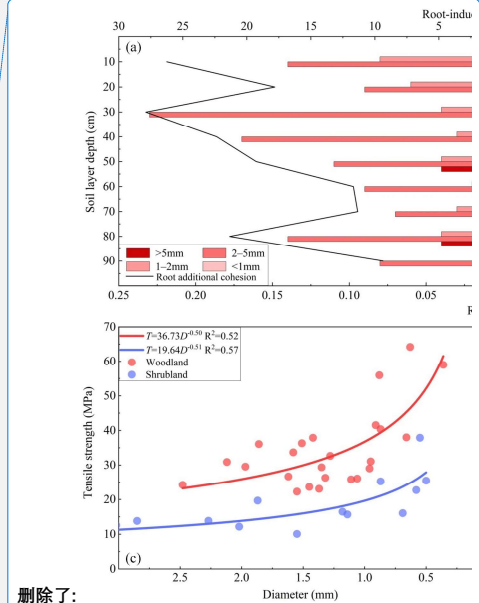
删除了: woodland

删除了:

设置了格式: 字体: 倾斜

设置了格式: 字体: 倾斜

设置了格式: 字体: 倾斜



删除了:

设置了格式: 字体: 倾斜

设置了格式: 字体: 倾斜

删除了: whiskers

删除了: are

K (mm·h ⁻¹)	Hydraulic conductivity	2.10	0.94
---------------------------	------------------------	------	------

414 5 Discussion

415 Long-term vegetation restoration policies may result in the dominant soil erosion process shift from traditional
 416 wind and water erosion to landslides (Deng et al., 2022; Yang et al., 2024; Du et al., 2025; Liao et al., 2025).
 417 Ecological restoration forests not only increase surface cover, but ~~the recovered vegetation extends~~ their root systems
 418 into potential sliding layers, thereby substantially altering slope hydrological processes and mechanical properties,
 419 and ~~playing~~ an important role in landslide initiation (Zhao et al., 2022; Cai et al., 2024; Chen et al., 2024; Lann et
 420 al., 2024). In this context, ~~our results highlight the hydro-mechanical heterogeneity across the Robinia~~
 421 ~~pseudoacacia – dominated woodland and Rosa xanthina – dominated shrubland, and assessed its influence on~~
 422 ~~landslide initiation.~~

423 The results of SWCC and HCF agree well with the infiltration patterns observed in dye-tracer experiments. In
 424 woodland soils, continuous preferential flow channels promote rapid infiltration, substantial downward water
 425 migration, and a high capacity for water storage and drainage. Shrubland soils exhibit scattered preferential flow
 426 channels, shorter infiltration pathways, pronounced shallow saturation, and a weaker capacity for water
 427 redistribution. The stained area ratio and patch distribution further corroborate these differences. Woodland profiles
 428 display vertical and continuous stained bands with greater infiltration depths, whereas shrubland profiles show
 429 shallow staining. This comparison indicates that variations in root distribution and diameter modify soil pore
 430 structure and thereby affect infiltration (Guan et al., 2024; Lann et al., 2024). Woodland soil with coarse roots and
 431 higher porosity facilitate deeper infiltration, whereas shrubland soils with shallow root systems provide lower
 432 infiltration capacity (Souza et al., 2023; Xiao et al., 2024; Hu et al., 2025). Preferential flow may result in the excess
 433 soil water storage over the rainfall depth, and the results from monitoring multiple natural rainfall events between
 434 20 May and 6 July 2023 further corroborate the assumption. In shrubland, soil moisture typically exhibits a delayed
 435 and attenuated response to rainfall. R_c values are consistently below zero, indicating low rainfall conversion
 436 efficiency. Most rainwater does not infiltrate but instead runs off once shallow soils saturate rapidly. In contrast,
 437 once rainfall over woodland slopes reaches a certain intensity, R_c values become positive. This pattern suggests that
 438 woodland slopes effectively intercept and infiltrate rainfall, sustain deeper water storage, and delay the development
 439 of saturation zones. This discrepancy is also evident in the critical $a_{cr} \times R_t$ values. The failure resistance on
 440 woodland slopes is higher than shrubland slopes, which may explain the contrasting distribution patterns observed
 441 in landslide number and size.

442 Vegetation-based slope protection has long been regarded as a key measure in traditional soil and water
 443 conservation, yet multidisciplinary studies have revealed its dual effects (Gyssels et al., 2005; Sidle and Bogaard,
 444 2016; Lann et al., 2024). Some herbaceous plants with shallow root systems can promote rapid surface saturation
 445 during intense rainfall, thereby enhancing hillslope runoff and rill erosion (Gong et al., 2024). Certain fast-growing
 446 tree species with shallow root systems may provide only limited soil reinforcement and thus increase the risk of
 447 shallow landslides (Ghestem and Sidle, 2011; Lin et al., 2024). Moreover, excessively thick litter layers can impede
 448 infiltration during short-duration storms and accelerate runoff concentration (Zhou et al., 2018; Rajão et al., 2023).
 449 These observations indicate that vegetation-based measures are not universally effective for soil erosion control
 450 (Löbmann et al., 2020; Lann et al., 2024). Our results further support this understanding. Shallow landslide initiation
 451 depends not only on rainfall but also on vegetation type, which modifies coupled hydrological-mechanical processes
 452 on slopes. ~~The deep root systems and stable preferential flow channels in woodland slopes may provide greater~~
 453 ~~resilience against slope failure compared to shrubland slopes.~~ This finding provides empirical evidence for forest-
 454 type allocation in ecologically sensitive areas. It also highlights the need for appropriate vegetation-type selection

删除了: extend

删除了: acting as

设置了格式: 字体: 倾斜

设置了格式: 字体: 倾斜

删除了: we focused the landslide initiation difference in two representative restoration forests from the hillslope hydrology and failure resistance heterogeneity.

删除了:

删除了: Woodland slopes, with deep root systems and stable preferential flow channels, enhance slope stability, whereas shrubland slopes, limited by shallow root systems, are more prone to rapid surface failure

465 and matching in regional soil and water conservation.

466 6 Conclusions

467 Vegetation recovery on the Chinese Loess Plateau has altered the dominant soil erosion process from runoff-
468 driven erosion to gravity-driven mass movements. Though previous studies have extensively investigated vegetation
469 effects on soil erosion, the specific role of vegetation in landslide initiation remains poorly understood. In this study,
470 we systematically examined landslide initiation processes in two contrasting vegetated landscapes: *Robinia*
471 *pseudoacacia* - dominated woodlands and *Rosa xanthina* - dominated shrublands, focusing on hydro-mechanical
472 heterogeneity. Following results can be drawn:

473 1. Landslides in woodland and shrubland exhibit obvious differences in initiation, depth and number. Shrubland
474 has a higher density of small, shallow landslides, whereas woodland has fewer but deeper and larger failures. This
475 contrast reflects a high-initiation-threshold and deep-seated-failure regime in woodland.

476 2. In shrubland, a loose, discontinuous pore system and pronounced hysteresis concentrate moisture in shallow
477 layers, causing rapid shallow saturation and large rainfall losses. In woodland, stable preferential flow paths promote
478 deeper and more efficient moisture migration, as reflected in higher soil water response index.

479 3. Woodland roots extend deeper and span a wider depth range than shrubland roots. Within the same depth
480 interval, root additional cohesion and *RAR* are also higher than those in shrubland. These patterns indicate stronger
481 root-network reinforcement in woodland soils and lower susceptibility to shallow landslides than in shrubland.
482 Therefore, the sediment production from landslide erosion may differ in various forest types, which has been rarely
483 addressed and deserves further study in future.

484 Acknowledgments

485 This research has been supported by the State Key Program of Natural Science of China (grant no. 42130701), and
486 the Natural Science Foundation of China (grant no. 42177309). The authors extend their gratitude to personnel at
487 the Jixian National Ecosystem Research Station of Shanxi Province, Beijing Forestry University, for their help during
488 field investigations.

489 Code and data availability

490 The corresponding author, Prof. Chao Ma, is willing to share the raw/processed data upon reasonable request.

491 Author contributions

492 Prof. Ma conceived the study based on his expertise in shallow landslides and unsaturated soil mechanics, and
493 proposed the concept of hydrological and hydromechanical coupling for analyzing vegetation-related slope
494 instability. Under the guidance of Prof. Ma, Ruijie Yang conducted soil hydrology experiments and drafted the
495 manuscript. Xi Yang and Xinying Wang assisted with field investigations. Yan Zang and Liqun Lyu contributed
496 research progress on shallow landslides and vegetation-slope interactions in the study area.

497 Competing interests

498 The authors declare no conflicts of interest.

499 References

500 An, J., Gao, G., Yuan, C., and Fu, B.: Inter- and intra-event rainfall partitioning dynamics of two typical xerophytic
501 shrubs in the loess plateau of china, Hydrology and Earth System Sciences Discussions, 26, 3885-3900,

删除了: in

删除了: may cause the dominant soil erosion process shift from runoff drive to gravitational attraction, while their role on landslide initiation hasn't been addressed.

删除了: work

删除了: addressed

删除了: the landslide initiation in woodland

设置了格式: 字体: 倾斜

删除了: shrubland

删除了:

设置了格式: 字体: 倾斜

删除了: by landslide spatial patterns, hydrological response, and slope failure resistance. Following results can be drawn

删除了: :

删除了: ,

删除了: values

设置了格式: 字体: 倾斜

删除了: Woodland roots concentrated at 10–25 cm provides greater root cohesion, greater slope failure resistance, and higher slope stability than shrubland roots confined to 0–10 cm depth. Therefore, the sediment production from landslide erosion in Chinese Loess Plateau may differ in various forest types, which deserves further study in future.

522 <https://doi.org/10.5194/hess-26-3885-2022>, 2022.

523 Bachmair, S., Weiler, M., and Troch, P. A.: Intercomparing hillslope hydrological dynamics: spatio-temporal
524 variability and vegetation cover effects, *Water Resour. Res.*, 48, W5537, <https://doi.org/10.1029/2011WR011196>,
525 2012.

526 Bai, R., Wang, X., Li, J., Yang, F., Shangguan, Z., and Deng, L.: The impact of vegetation reconstruction on soil
527 erosion in the loess plateau, *J. Environ. Manage.*, 363, 121382, <https://doi.org/10.1016/j.jenvman.2024.121382>,
528 2024.

529 Borrelli, P., Robinson, D. A., Panagos, P., Lugato, E., Yang, J. E., Alewell, C., Wuepper, D., Montanarella, L., and
530 Ballabio, C.: Land use and climate change impacts on global soil erosion by water (2015-2070), *Proc. Natl. Acad.*
531 *Sci. U. S. A.*, 117, 21994-22001, <https://doi.org/10.1073/pnas.2001403117>, 2020.

532 Cai, L., Wang, F., Lin, Y., Long, Q., Zhao, Y., Han, J., Ge, W., and Chen, H.: Changes in preferential flow caused
533 by root effects in black locust plantations of different stand ages in the semi-arid region of the loess plateau, *J.*
534 *Hydrol.*, 634, 131086, <https://doi.org/10.1016/j.jhydrol.2024.131086>, 2024.

535 Chen, M., Yang, X., Zhang, X., Bai, Y., Shao, M., Wei, X., Jia, Y., Wang, Y., Jia, X., Zhu, Y., Zhang, Q., Zhu, X.,
536 and Li, T.: Response of soil water to long-term revegetation, topography, and precipitation on the chinese loess
537 plateau, *Catena*, 236, 107711, <https://doi.org/10.1016/j.catena.2023.107711>, 2024.

538 Deng, J., Ma, C., and Zhang, Y.: Shallow landslide characteristics and its response to vegetation by example of july
539 2013, extreme rainstorm, central loess plateau, china, *Bull. Eng. Geol. Environ.*, 81, 100, <https://doi.org/10.1007/s10064-022-02606-1>, 2022.

541 Dibiagio, A., Capobianco, V., Oen, A., and Tallaksen, L. M.: State-of-the-art: parametrization of hydrological and
542 mechanical reinforcement effects of vegetation in slope stability models for shallow landslides, *Landslides*, 21,
543 2417-2446, <https://doi.org/10.1007/s10346-024-02300-1>, 2024.

544 Du, P., Chen, Y., Zhao, Y., Qu, L., Liu, H., Liu, Z., Xu, J., and Tian, X.: Formation process and depositional
545 characteristics of mudballs in the loess plateau during extreme rainstorms: dual-threshold constraints on material
546 sources and dynamic conditions, *J. Environ. Manage.*, 391, 126590, [https://doi.org/10.1016/j.jenvman.2025.](https://doi.org/10.1016/j.jenvman.2025.126590)
547 126590, 2025.

548 Fan, L., Lehmann, P., Zheng, C., and Or, D.: Rainfall intensity temporal patterns affect shallow landslide triggering
549 and hazard evolution, *Geophys. Res. Lett.*, 47, e2019GL085994, [https://doi.org/https://doi.org/10.1029/2019GL](https://doi.org/https://doi.org/10.1029/2019GL085994)
550 085994, 2020.

551 Feng, X., Fu, B., Piao, S., Wang, S., Ciais, P., Zeng, Z., Lü, Y., Zeng, Y., Li, Y., Jiang, X., and Wu, B.: Revegetation
552 in china's loess plateau is approaching sustainable water resource limits, *Nat. Clim. Chang.*, 6, 1019-1022,
553 <https://doi.org/10.1038/nclimate3092>, 2016.

554 Franklin, S. M., Kravchenko, A. N., Vargas, R., Vasilas, B., Fuhrmann, J. J., and Jin, Y.: The unexplored role of
555 preferential flow in soil carbon dynamics, *Soil Biology and Biochemistry*, 161, 108398, [https://doi.org/10.1016/](https://doi.org/10.1016/j.soilbio.2021.108398)
556 j.soilbio.2021.108398, 2021.

557 Fu, B., Wang, S., Liu, Y., Liu, J., Liang, W., and Miao, C.: Hydrogeomorphic ecosystem responses to natural and
558 anthropogenic changes in the loess plateau of china, *Annual Review of Earth & Planetary Sciences*, 45, 223-243,
559 <https://doi.org/10.1146/annurev-earth-063016-020552>, 2016.

560 Ghestem, M. and Sidle, R.: The influence of plant root systems on subsurface flow: implications for slope stability,
561 *Bioscience*, 61, 869-879, <https://doi.org/10.1525/bio.2011.61.11.6>, 2011.

562 Gong, C., Ni, D., Liu, Y., Li, Y., Huang, Q., Tian, Y., and Zhang, H.: Herbaceous vegetation in slope stabilization:
563 a comparative review of mechanisms, advantages, and practical applications, *Sustainability*, 16, 7620,
564 <https://doi.org/10.3390/su16177620>, 2024.

565 Gu, C., Mu, X., Gao, P., Zhao, G., Sun, W., Tatarko, J., and Tan, X.: Influence of vegetation restoration on soil
566 physical properties in the loess plateau, china, *J. Soils Sediments*, 19, 716-728, [https://doi.org/10.1007/s11368-](https://doi.org/10.1007/s11368-018-2083-3)
567 018-2083-3, 2019.

568 Guan, N., Bi, H., Song, Y., Lu, S., Lin, D., and Han, J.: Vegetation restoration is affecting the characteristics and
569 patterns of infiltration in the loess plateau, *Catena*, 243, 108190, <https://doi.org/10.1016/j.catena.2024.108190>,
570 2024.

571 Gyssels, G., Poesen, J., Bochet, E., and Li, Y.: Impact of plant roots on the resistance of soils to erosion by water: a
572 review, *Progress in Physical Geography*, 29, 189-217, <https://doi.org/10.1191/0309133305pp443ra>, 2005.

573 Hao, M., Jin, Z., Luo, D., Cao, G., Jiang, C., Han, H., Yang, S., and Zhang, J.: Rainstorm erosion difference and
574 topographical changes induced by heavy rainfall between afforestation and grassland restoration catchments on
575 the chinese loess plateau, *Geomorphology*, 457, 109243, <https://doi.org/10.1016/j.geomorph.2024.109243>, 2024.

576 Hu, J., Ren, Y., Tang, M., Zhang, Z., Yang, K., Zhen, Q., and Han, F.: Effects of vegetation restoration on infiltration
577 patterns and preferential flow in semi-arid areas with shallowly buried soft bedrock (pisha sandstone) in china, *J.*
578 *Hydrol.*, 661, 133546, <https://doi.org/10.1016/j.jhydrol.2025.133546>, 2025.

579 Lan, H., Zhao, X., Macciotta, R., Peng, J., Li, L., Wu, Y., Zhu, Y., Liu, X., Zhang, N., and Liu, S.: The cyclic
580 expansion and contraction characteristics of a loess slope and implications for slope stability., *Sci. Rep.*, 11, 2250,
581 <https://doi.org/10.1038/s41598-021-81821-4>, 2021.

582 Lann, T., Bao, H., Lan, H., Zheng, H., Yan, C., and Peng, J.: Hydro-mechanical effects of vegetation on slope
583 stability: a review, *Sci. Total Environ.*, 926, 171691, <https://doi.org/10.1016/j.scitotenv.2024.171691>, 2024.

584 Laycock, W. A., Geological Survey U. S., I. B., New, J. D. O. W., United, S. F. S., and Rutgers, U. (Eds.):
585 Distribution of roots and rhizomes in different soil types in the pine barrens of new jersey, U.S. Geological Survey
586 Professional Paper, Washington, 1967.

587 Li, F., Song, X., Tang, C., Liu, C., Yu, J., and Zhang, W.: Tracing infiltration and recharge using stable isotope in
588 taihang mt., North china, *Environmental Geology*, 53, 687-696, <https://doi.org/10.1007/s00254-007-0683-0>, 2007.

589 Li, J., Cui, P., and Yin, Y.: Field observation and micro-mechanism of roots-induced preferential flow by infiltration
590 experiment and phase-field method, *J. Hydrol.*, 623, 129756, <https://doi.org/10.1016/j.jhydrol.2023.129756>, 2023.

591 Li, P., Pan, Z., Xiao, T., and Wang, J.: Effects of molding water content and compaction degree on the microstructure
592 and permeability of compacted loess, *Acta Geotech.*, 18, 921-936, <https://doi.org/10.1007/s11440-022-01592-8>,
593 2023.

594 Li, S., Zheng, C., Lu, T., Zhou, K., Gu, Y., Wang, B., and Lu, Y.: Characteristics and influencing factors of loess
595 terraces' preferential flow under different typical vegetation cover, *Plant Soil*, in press, [https://doi.org/10.1007/](https://doi.org/10.1007/s11104-025-07710-1)
596 s11104-025-07710-1, 2025.

597 Liang, H., Li, Y., An, X., Liu, J., Pan, N., and Li, Z.: Soil moisture dynamics and its temporal stability under
598 different-aged caragana korshinskii shrubs in the loess hilly region of china, *Water*, 15, 2334, [https://doi.org/](https://doi.org/10.3390/w15132334)
599 10.3390/w15132334, 2023.

600 Liao, J., Wang, J., Jiao, J., Yan, Z., Li, J., Zhang, Z., Li, M., Xu, Q., Jiang, X., Zhao, W., Ling, Q., Sheng, H., Chen,
601 Y., and Wu, T.: Rusle tends to overestimate soil erosion in revegetated conditions: evidence from long-term runoff
602 plots monitoring on china's loess plateau, *Catena*, 258, 109285, <https://doi.org/10.1016/j.catena.2025.109285>,
603 2025.

604 Lin, Y., Jian, W., Wu, Y., Zhu, Z., Wang, H., Dou, H., and Lai, Z.: Effect of tree roots on heavy rainfall-induced
605 shallow landslides, *Geomatics, Natural Hazards and Risk*, 15, 2360002, [https://doi.org/10.1080/19475705.2024.](https://doi.org/10.1080/19475705.2024.2360002)
606 2360002, 2024.

607 Liu, X., Feng, T., Zhang, Y., Liu, Y., and Wang, P.: Vegetation restoration affects soil hydrological processes in

608 typical natural and planted forests on the loess plateau, *J. Hydrol.*, 650, 132465, [https://doi.org/10.1016/j.jhydrol.](https://doi.org/10.1016/j.jhydrol.2024.132465)
609 2024.132465, 2025.

610 Löbmann, M. T., Geitner, C., Wellstein, C., and Zerbe, S.: The influence of herbaceous vegetation on slope stability
611 – a review, *Earth-Sci. Rev.*, 209, 103328, <https://doi.org/10.1016/j.earscirev.2020.103328>, 2020.

612 Lu, N. and Godt, J. W. (Eds.): *Hillslope hydrology and stability*, Cambridge University Press, Cambridge, U.K.,
613 2013.

614 Lu, N., Calderon, A. R. A., Waylace, A., Lovekin, J., and Crandall, A.: Suction stress-based rainfall intensity-
615 duration method for slope instability prediction, *J. Geotech. Geoenviron. Eng.*, 150, 4024069, [https://doi.org/](https://doi.org/10.1061/JGGEFK.GTENG-12597)
616 10.1061/JGGEFK.GTENG-12597, 2024.

617 Masi, E. B., Tofani, V., Rossi, G., Cuomo, S., Wu, W., Salciarini, D., Caporali, E., and Catani, F.: Effects of roots
618 cohesion on regional distributed slope stability modelling, *Catena*, 222, 106853, [https://doi.org/10.1016/j.catena.](https://doi.org/10.1016/j.catena.2022.106853)
619 2022.106853, 2023.

620 Montgomery, D. R. and Dietrich, W. E.: A physically based model for the topographic control on shallow landsliding,
621 *Water Resour. Res.*, 30, 1153-1171, <https://doi.org/10.1029/93WR02979>, 1994.

622 Montgomery, D. R. and Dietrich, W. E.: Landscape dissection and drainage area-slope thresholds, in: *Process*
623 *Models and Theoretical Geomorphology*, edited, John Wiley & Sons, Chichester, 221-246, 1994.

624 Montgomery, D. R., Schmidt, K. M., Greenberg, H. M., and Dietrich, W. E.: Forest clearing and regional landsliding,
625 *Geology*, 28, 311-314, [https://doi.org/10.1130/0091-7613\(2000\)28<311:FCARL>2.0.CO;2](https://doi.org/10.1130/0091-7613(2000)28<311:FCARL>2.0.CO;2), 2000.

626 Nimmo, J. R., Perkins, K. S., Schmidt, K. M., Miller, D. M., Stock, J. D., and Singha, K.: Hydrologic characterization
627 of desert soils with varying degrees of pedogenesis: 1. Field experiments evaluating plant-relevant soil water
628 behavior, *Vadose Zone J.*, 8, 480-495, <https://doi.org/10.2136/vzj2008.0052>, 2009.

629 Niu, F., Pan, C., and Cui, Y.: Experimental investigation to the effect of different land-use on rainfall infiltration
630 runoff patterns and preferential flow distribution in the loess area of western shanxi province, *Acta Ecologica*
631 *Sinica*, 43, 4144-4166, <https://doi.org/10.5846/stxb202204130989>, 2023.

632 Rajão, P., Berg, M., Cornelissen, J., and Dias, A.: The effects of leaf traits on litter rainfall interception with
633 consequences for runoff and soil conservation, *J. Ecol.*, 111, 2662-2675, <https://doi.org/10.1111/1365-2745.14203>,
634 2023.

635 Schwarz, M., Preti, F., Giadrossich, F., Lehmann, P., and Or, D.: Quantifying the role of vegetation in slope stability:
636 a case study in tuscany (italy), *Ecol. Eng.*, 36, 285-291, <https://doi.org/10.1016/j.ecoleng.2009.06.014>, 2010.

637 Sidle, R. C. and Bogaard, T. A.: Dynamic earth system and ecological controls of rainfall-initiated landslides, *Earth-*
638 *Sci. Rev.*, 159, 275-291, <https://doi.org/10.1016/j.earscirev.2016.05.013>, 2016.

639 Souza, L. F. T., Hirmas, D. R., Sullivan, P. L., Reuman, D. C., Kirk, M. F., Li, L., Ajami, H., Wen, H., Sarto, M. V.
640 M., Loecke, T. D., Rudick, A. K., Rice, C. W., and Billings, S. A.: Root distributions, precipitation, and soil
641 structure converge to govern soil organic carbon depth distributions, *Geoderma*, 437, 116569,
642 <https://doi.org/10.1016/j.geoderma.2023.116569>, 2023.

643 Tang, B., Jiao, J., Zhang, Y., Chen, Y., Wang, N., and Bai, L.: The magnitude of soil erosion on hillslopes with
644 different land use patterns under an extreme rainstorm on the northern loess plateau, china, *Soil and Tillage*
645 *Research*, 204, 104716, <https://doi.org/10.1016/j.still.2020.104716>, 2020.

646 Tang, P., Zhang, J., Li, Y., Wei, G., Hu, Y., and Zhao, J.: Effects of extreme rainfall on the morphological
647 characteristics and spatial distribution of shallow landslides under different land use patterns in the loess region of
648 western shanxi province, northern china, *Journal of Beijing Forestry University*, 45, 109-117, [https://doi.org/10.](https://doi.org/10.12171/j.1000-1522.20230070)
649 12171/j.1000-1522.20230070, 2023.

650 Wang, N. and Zhang, T.: Soil pore structure and its research methods: a review, *Soil Water Res.*, 19, 1-24,

651 <https://doi.org/10.17221/64/2023-SWR>, 2024.

652 Wang, R., Dong, Z., Zhou, Z., Wang, N., Xue, Z., and Cao, L.: Effect of vegetation patchiness on the subsurface
653 water distribution in abandoned farmland of the loess plateau, china, *Sci. Total Environ.*, 746, 141416,
654 <https://doi.org/10.1016/j.scitotenv.2020.141416>, 2020.

655 Wang, R., Dong, Z., Zhou, Z., and Wang, P.: Temporal variation in preferential water flow during natural vegetation
656 restoration on abandoned farmland in the loess plateau of china, *Land*, 8, 186, <https://doi.org/10.3390/land8120186>, 2019.

657

658 Wang, X., Ma, C., Lyu, L., and Zhang, Y.: Erosion characteristics of shallow landslides undervarious land-use
659 conditions: an example of the caijiachuan landslide, *Arid Zone Research*, 41, 697-705,
660 <https://doi.org/10.13866/j.azr.2024.04.15>, 2024.

661 Wang, Y., Dong, G., Qu, L., Wu, Z., Zhao, F., and Shao, C.: Ecosystem functioning of the loess plateau in china
662 from vegetation restoration relied largely on climate, *Forests*, 14, 27, <https://doi.org/10.3390/f14010027>, 2022.

663 Wei, Y. Z., Yao, Z. H., Chong, X. L., Zhang, J. H., and Zhang, J.: Microstructure of unsaturated loess and its
664 influence on strength characteristics, *Sci. Rep.*, 12, 1502, <https://doi.org/10.1038/s41598-022-05464-9>, 2022.

665 Wen, S., Shao, M., and Wang, J.: Earthworm burrowing activity and its effects on soil hydraulic properties under
666 different soil moisture conditions from the loess plateau, china, *Sustainability*, 12, 9303, <https://doi.org/10.3390/su12219303>, 2020.

667

668 Xiao, T., Li, P., Fei, W., and Wang, J.: Effects of vegetation roots on the structure and hydraulic properties of soils:
669 a perspective review, *Sci. Total Environ.*, 906, 167524, <https://doi.org/10.1016/j.scitotenv.2023.167524>, 2024.

670 Xu, P., Zhang, Q., Qian, H., Li, M., and Yang, F.: An investigation into the relationship between saturated
671 permeability and microstructure of remolded loess: a case study from chinese loess plateau, *Geoderma*, 382,
672 114774, <https://doi.org/10.1016/j.geoderma.2020.114774>, 2021.

673 Yamase, K., Ikeno, H., Hotta, N., Imawaka, M., Ohashi, M., Tanikawa, T., Todo, C., Dannoura, M., and Hirano, Y.:
674 Effect of sprouting and corresponding root distribution of the shrub species eurya japonica on slope stability,
675 *Catena*, 238, 107869, <https://doi.org/10.1016/j.catena.2024.107869>, 2024.

676 Yan, X., Nunes, J. P., Sun, J., Tang, D., Wen, Y., and Li, Z.: Restored vegetation dominates the decrease in surface
677 and subsurface runoff on the loess plateau, *J. Hydrol.*, 640, 131730, <https://doi.org/10.1016/j.jhydrol.2024.131730>,
678 2024.

679 Yang, B., Jiao, J., Ma, X., Zhao, W., Ling, Q., Zhang, X., Han, J., Du, P., Chen, Y., and Chen, H.: Distribution and
680 formation of soil balls under heavy rainstorm conditions in the northern loess plateau, *J. Hydrol.*, 625, 130103,
681 <https://doi.org/10.1016/j.jhydrol.2023.130103>, 2023.

682 Yang, B., Ma, X., Jiao, J., Zhao, W., Ling, Q., Li, J., and Zhang, X.: Magnitude and hotspots of soil erosion types
683 during heavy rainstorm events on the loess plateau: implications for watershed management, *Catena*, 246, 108365,
684 <https://doi.org/10.1016/j.catena.2024.108365>, 2024.

685 Zhang, S., Liu, Y., Yang, M., Tian, P., Mu, X., and Zhao, G.: Impact of vegetation restoration on preferential flow
686 and soil infiltration capacity in the hilly region of the loess plateau, *Journal of Hydrology: Regional Studies*, 59,
687 102333, <https://doi.org/10.1016/j.ejrh.2025.102333>, 2025.

688 Zhang, Y., Tang, Z., Zhang, J., Zhang, Z., and Zhang, M.: Visualizing preferential flow paths using dye tracer and
689 species diversity theory methods to explore their correlation to soil properties with random forest algorithm, *J.*
690 *Hydrol.*, 638, 131570, <https://doi.org/10.1016/j.jhydrol.2024.131570>, 2024.

691 Zhao, M., Li, D., Huang, Y., Deng, Y., Yang, G., Lei, T., and Huang, Y.: Soil matrix infiltration characteristics in
692 differently aged eucalyptus plantations in a southern subtropical area in china, *Catena*, 217, 106490,
693 <https://doi.org/10.1016/j.catena.2022.106490>, 2022.

694 Zhou, Q., Zhou, X., Luo, Y., and Cai, M.: The effects of litter layer and topsoil on surface runoff during simulated
695 rainfall in guizhou province, china: a plot scale case study, *Water*, 10, 915, <https://doi.org/10.3390/w10070915>,
696 2018.
697